JOURNAL OF Materials CHEMISTRY

Structural aspects of a series of cation radical salts of tetrathiotetracene (TTT) with 2-alkoxy-1,1,3,3-tetracyanoallyl anions (RO-TCA$^-$; R = Me, Et, Pr^n, Bu^n)†

Shuichi Sekizaki,*[a] Chiyoko Tada,[a] Hideki Yamochi[a,b] and Gunzi Saito*[a]

[a]*Division of Chemistry, Graduate School of Science, Kyoto University, Sakyo-ku, Kyoto 606-8502, Japan. E-mail: sekizaki@kuchem.kyoto-u.ac.jp; saito@kuchem.kyoto-u.ac.jp*
[b]*CREST, Japan Science and Technology Corporation (JST)*

Received 14th June 2001, Accepted 19th June 2001
First published as an Advance Article on the web 31st July 2001

Eight cation radical salts of tetrathiotetracene‡ (TTT) with a series of 2-alkoxytetracyanoallyl anions (RO-TCA$^-$; R = Me, Et, Pr^n, Bu^n) were prepared by electrocrystallisation. All of them were non-magnetic semiconductors. Seven crystal structures were determined. The physical and structural aspects of the salts were well categorised by their stoichiometries of donor to anion, 3 : 2, 1 : 1 and 1 : 2. The 1 : 2 salts had alternating stacks of dication of TTT and anion molecules, which is uncommon for TTT salts. Molecular structures were also studied by PM3 and RHF/6-31G* calculations. One of the fascinating features of RO-TCAs is their structural flexibility, which gives rise to multiple stoichiometries with varied physical properties.

1 Introduction

Tetrathiotetracene‡ (or tetrathionaphthacene, abbreviated as TTT, Fig. 1) is known as a stronger donor than most tetrathiafulvalene (TTF) derivatives.[1] It gives highly conducting cation radical salts with inorganic counter anions in the partial charge transfer (CT) state (TTT$^{\gamma+}$, $0 < \gamma < 1$)(γ: degree of CT), *e.g.* $(TTT)_2I_3$ ($\sigma_{rt} \approx 10^3$ S cm^{-1}, where σ_{rt} is electric conductivity at room temperature). CT complexes based on TTT were investigated mainly before the discovery of organic superconductors based on TTF derivatives; however, for several years, TTT derivatives have attracted notice again as non-TTF-type donors. Some of the salts based on them were reported to show a noteworthy feature: some 1 : 1 cation radical salts based on DMTSA, in which donor molecules are fully ionised ($\gamma = 1$), show metallic behaviour.[2] The chemical structures in the text are depicted in Fig. 1.

To explore such novel salts or a wide variety of crystal structures and physical properties, one of the effective ways is the use of organic counter anions instead of inorganic ones because of the ability to design the shape, size and charge of the organic molecules. The organic anions are also expected to stabilise metallic states by means of their large polarisabilities.[3] Furthermore, the introduction of heteroatoms to the anions may increase the dimensionality of the salts and/or build some kinds of supramolecular network owing to atomic contacts between donor and anion molecules. Considering these points, we have investigated cation radical salts with cyanocarbons, mainly 1,1,3,3-tetracyanoallyl anion (TCA$^-$) derivatives such as PCA$^-$, HCTMM^{2-} and DHCP^{2-} (ref. 4).

In this study, the title anions, a series of 2-alkoxy-1,1,3,3-TCA anion (RO-TCA$^-$; R = methyl, ethyl, *n*-propyl, *n*-butyl), are chosen from the following viewpoints: (1) a feature of RO-TCAs is that the sizes can be easily changed by substituting the alkyl groups without changes of the formal charge; (2) they have flexible molecular structures and hence are expected to afford polymorphic salts with a given donor. We describe the preparation, crystal and molecular structures and physical properties of TTT salts with RO-TCA,[5] with consideration of the flexibility of the RO-TCA anions. Especially, we place emphasis on the structures of the component molecules in order to understand their fundamental features.

2 Experimental

Materials

TTT was prepared according to the literature[6] and purified by recrystallisation followed by gradient sublimation.

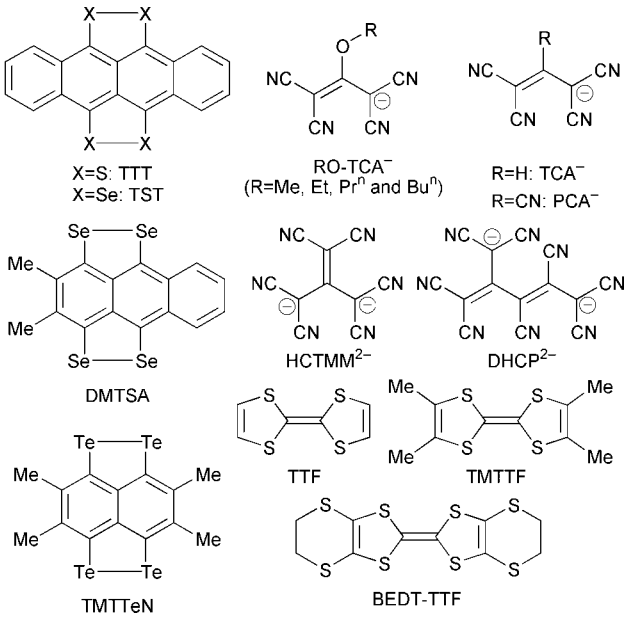

Fig. 1 Molecules discussed in the text.

†Electronic supplementary information (ESI) available: further experimental details for compounds **1**–**4** and **6**–**8**. See http://www.rsc.org/suppdata/jm/b1/b105340j/

‡The IUPAC name for tetrathiotetracene is tetraceno[5,6-*cd*:11,12-*c′d′*]bis[1,2]dithiole.

Table 1 Conditions of electrocrystallisation

	Anion	Donor : anion	Appearance	Donor/mg	Electrolytes[d]/mg	Solvent, amount/mL
1	MeO-TCA	1 : 1[ab]	Black needles	10	41	THF, 18
2	EtO-TCA	1 : 1 : 0.25(THF)[ab]	Black needles	10	45	THF, 18
3	EtO-TCA	1 : 2[b]	Black elongated plates	4	45	THF, 18 or $PhNO_2$, 18
4	PrO-TCA	1 : 1 : 0.5(THF)[ab]	Black plates	4	45	THF, 18
5	PrO-TCA	—[c]	Black needles	5	45	THF, 18
6	PrO-TCA	3 : 2[ab]	Black needles	10	45	THF, 18
7	PrO-TCA	1 : 2[b]	Black elongated plates	4	45	THF, 17 + EtOH, 1
8	BuO-TCA	1 : 1[ab]	Black needles	10	45	THF, 18

[a]Determined by elemental analysis. [b]Determined by X-ray crystal structure analysis, and observed density by the floating method. [c]Not determined because of low yield and low quality of the crystal. [d]Tetrabutylammonium (TBA) salts were used for Me, Et and PrO-TCA, and tetrapropylammonium (TPA) salt for BuO-TCA.

$(TTT)Cl{\cdot}H_2O$, $(TTT)(HSO_4)_2$ and $(TTT)Br_2$ were prepared according to the literature.[7]

Tetraalkylammonium salts of MeO-TCA and EtO-TCA were synthesised by the procedures in ref. 8. Those of PrO-TCA and BuO-TCA were similarly synthesised as described in the Electronic Supplementary Information.†

Cation radical salts were obtained by electrooxidation of TTT in the presence of the tetraalkylammonium salt of the RO-TCA from tetrahydrofuran (THF), THF–ethanol (EtOH) or nitrobenzene ($PhNO_2$) in H-shaped cells equipped with platinum electrodes. The applied current was 0.5 μA (*ca.* 0.2 μA cm^{-2}) for 40–50 days in all cases. Most of the salts were grown on the surface of undissolved TTT in the cells. Although polymorphism was realised in the combinations of TTT and RO-TCA (R = Et, Pr), only one phase of the salts could be obtained in a batch in most cases. The salts and residual donor were separated under a microscope on the basis of their external morphology. The detailed conditions of the electrocrystallisation are summarised in Table 1. From now on, the salts will be referred to by the numbers in the first column of Table 1. The stoichiometries were determined by elemental analyses and/or X-ray crystal structure analyses. However, the composition of **5** was not determined because of its low yield and low quality of the crystals.

Measurements

Cyclic voltammetric measurements were performed in 0.1 M solutions of tetrabutylammonium tetrafluoroborate ($TBA{\cdot}BF_4$) in acetonitrile with Pt electrodes *vs.* SCE (saturated calomel electrode) at a scan speed of 10 mV s^{-1} using a Yanaco Polarographic Analyser P-1100 at 20–22 °C. The redox potential of TTT was measured on $(TTT)Cl{\cdot}H_2O$ by the differential pulse method because of its low solubility.

Optical absorption spectra were measured on a Perkin-Elmer 1600 Series FT-IR spectrometer (resolution 4 cm^{-1}) for IR and near-IR (NIR) regions (400–7800 cm^{-1}) with KBr discs and on a Shimadzu UV-3100 spectrometer for the UV-Vis-NIR region (3800–4200 cm^{-1}) with KBr discs or solutions in quartz cells.

X-Ray reflection data for the structural analyses were collected at room temperature on automatic four circle diffractometers (MAC Science MXC series) or oscillator type imaging plate systems (MAC Science DIP series) with graphite monochromated Mo-Kα radiation. The crystal structures were solved by direct methods and refined by full matrix least squares.[9] Hydrogen atoms of TTT and MeO-TCA were determined by differential synthesis. Those of RO-TCAs with the other alkyl groups were calculated by assuming sp^3 configuration and C–H bond lengths of 0.96 Å. They were refined with isotropic thermal parameters, while non-hydrogen atoms were refined with anisotropic thermal parameters. THF molecules in **2** and **4** are located at the centres of inversion and disordered. The specific densities of the salts were measured by the floating method.

CCDC 165346–165352. See http://www.rsc.org/suppdata/jm/b1/b105340j/ for crystallographic files in .cif format.

Molecular orbital (MO) and intermolecular overlap integrals of highest occupied MOs (HOMOs) were calculated by extended Hückel methods with single-ζ Slater components including the 3d-orbitals of the sulfur atoms.[10] Geometry optimisations were performed by the semi-empirical PM3 method[11] and by *ab initio* restricted Hartree–Fock (RHF)[12] method with 6-31G* basis set.[13]

DC resistivities were measured by a two-probe method attaching gold wires (20 μm diameter) on the samples with gold paste (Tokuriki No. 8560-1A).

Static magnetic susceptibilities were measured on a SQUID magnetometer (Quantum Design MPMS2). Randomly oriented single crystals were wrapped in polyethylene film and held in a plastic straw during the measurements. Spin susceptibilities were corrected by subtracting the blank signals of the holder and core contributions of the components using Pascal's law.

3 Results and discussion

3.1 Redox properties and basicity of RO-TCA

Before describing the properties of the TTT salts, we will mention the redox properties and basicity of $RO\text{-}TCA^-$, because the charge of the anion determines those of the donor molecules which strongly influence the physical properties of the salts.

The redox processes of $RO\text{-}TCA^-$ anions are irreversible, and only oxidation peak potentials for the process of $RO\text{-}TCA^- \rightarrow RO\text{-}TCA^{\bullet}$ can be observed. Therefore, the peak potentials (E_p^{ox}) of $RO\text{-}TCA^-$ are compared with the first and second half wave redox potentials ($E_{1/2}^1$ and $E_{1/2}^2$) of TTT and some common TTF derivatives in Table 2, where $E_{1/2}^1$ and $E_{1/2}^2$

Table 2 Redox potential of donors and oxidation potential of RO-TCA[a]

	$E_{1/2}^1$/V ($D^0 \rightleftarrows D^{+\bullet}$)	$E_{1/2}^2$/V ($D^{+\bullet} \rightleftarrows D^{2+}$)		E_p^{ox}/V ($A^- \rightarrow A^{\bullet}$)
TTT[b]	+0.15	+0.51	TBA·MeO-TCA	+1.32
TMTTF	+0.29	+0.65	TBA·EtO-TCA	+1.30
TTF	+0.37	+0.76	TBA·PrO-TCA	+1.30
BEDT-TTF	+0.53	+0.78	TPA·BuO-TCA	+1.30

[a]Measured in 0.1 M acetonitrile solution of $TBA{\cdot}BF_4$ with Pt electrodes *vs.* SCE. [b]Measured on $(TTT)Cl{\cdot}H_2O$ by differential pulse method because of its low solubility.

Table 3 Crystallographic data of TTT salts

Salt (anion)	1 : 1 salts				1 : 2 salts		3 : 2 salt
D : A	**1** (MeO-TCA) 1 : 1	**2** (EtO-TCA) 1 : 1 : 0.25 (THF)	**8** (BuO-TCA) 1 : 1	**4** (PrO-TCA) 1 : 1 : 0.5 (THF)	**3** (EtO-TCA) 1 : 2	**7** (PrO-TCA) 1 : 2	**6** (PrO-TCA) 3 : 2
Formula	$C_{26}H_{11}N_4O_1S_4$	$C_{28}H_{15}N_4O_{1.25}S_4$	$C_{29}H_{17}N_4O_1S_4$	$C_{30}H_{19}N_4O_{1.5}S_4$	$C_{36}H_{18}N_8O_2S_4$	$C_{38}H_{22}N_8O_2S_4$	$C_{74}H_{38}N_8O_2S_{12}$
Formula weight	511.65	543.71	565.74	587.77	722.86	750.91	1455.96
Crystal system	Monoclinic	Triclinic	Monoclinic	Triclinic	Triclinic	Triclinic	Triclinic
Space group	$P2_1/n$	$P\bar{1}$	$C2/c$	$P\bar{1}$	$P\bar{1}$	$P\bar{1}$	$P\bar{1}$
a/Å	12.351(2)	7.573(1)	20.971(7)	11.969(2)	7.814(1)	7.915(2)	10.357(3)
b/Å	23.632(4)	14.909(1)	21.949(8)	12.060(2)	8.649(2)	8.736(4)	12.243(8)
c/Å	7.603(1)	23.061(2)	14.078(5)	11.166(2)	14.448(2)	14.680(4)	14.085(9)
α/°	—	74.423(4)	—	73.67(1)	105.06(1)	74.50(2)	74.74(5)
β/°	101.48(1)	88.636(5)	128.70(2)	84.16(1)	91.61(1)	75.25(2)	69.26(4)
γ/°	—	83.511(5)	—	59.910(8)	116.51(1)	64.59(2)	73.11(4)
V/Å^3	2174.9(6)	2491.3(1)	5057(3)	1336.8(5)	823.0(2)	872.0(5)	1573(2)
Z	4	4	8	2	1	1	1
μ(Mo-Kα)/cm^{-1}	4.465	3.948	3.914	3.742	3.189	3.070	4.559
No. of unique reflection	4986	9024	4049	4305	3821	3616	7220
No. of used reflection	2992 ($I > 3\sigma(I)$)	6515 ($I > 3\sigma(I)$)	2956 ($I > 3\sigma(I)$)	2829 ($I > 1.5\sigma(I)$)	2256 ($I > 3\sigma(I)$)	2584 ($I > 3\sigma(I)$)	3337 ($I > 3\sigma(I)$)
No. of parameters	360	770	375	414	242	251	481
R	0.041	0.039	0.048	0.083	0.049	0.050	0.050

are defined by the averaged potentials of the oxidation and reduction peak potentials corresponding to the processes of $D^0 \rightleftarrows D^{+\bullet}$ and $D^{+\bullet} \rightleftarrows D^{2+}$, respectively. The oxidation potentials of RO-TCA$^-$ anions are around +1.30 V *vs.* SCE regardless of the alkyl groups and are largely positive compared to the $E_{1/2}{}^1$ and $E_{1/2}{}^2$ values of TTT and TTF derivatives.

UV-Vis spectra of RO-TCA$^-$ anions in EtOH solution of hydrochloric acid (*ca.* 1 mol L^{-1}) are the same as that in pure EtOH. This result indicates that the basicities of the RO-TCA$^-$ anions are weaker than that of chloride,[14] because if RO-TCA$^-$ anions are protonated by any acids, their π-conjugated systems become short, and then their optical absorption bands must appear at higher energy than RO-TCA$^-$ anions themselves.

Consequently, RO-TCAs are expected to be very stable as monoanions towards both the protonation and the electrooxidation of the donor molecules in Table 2 within normal conditions of electrocrystallisation.

3.2 Crystal and molecular structures of TTT salts

General scope of crystal and molecular structures. Crystal data and experimental details are summarised in Table 3. The salts are categorised by the ratio of donor to anion, 1 : 1, 1 : 2 and 3 : 2. One of the structural characteristics is that, when the ratio is the same, the salts give similar packing of TTT molecules with one exception (salt **4**). In the 1 : 1 salts except for **4**, TTT molecules form segregated columns. The 3 : 2 salt also has segregated columns with charge separation. The other salts, **4** and the 1 : 2 salts, have alternating stacks. To our knowledge, TTT salts consisting of alternating stacks and structure of TTT^{2+} have not been reported so far.

In 1 : 1 and 3 : 2 salts, $TTT^{+\bullet}$ molecules form dimers. The intradimer and interdimer overlap modes of TTT molecules, interplanar distances, numbers of intermolecular short atomic contacts, and overlap integrals of HOMOs are summarised in Table 4. As shown schematically in Fig. 2, the overlap modes of TTT molecules so far observed including this work are roughly classified into five types on the basis of the slip of the molecular centre along the molecular long and short axes (x and y, respectively, indicated by arrows in Fig. 2). In types A and B, the molecules are shifted with respect to each other in the directions of x (~3.6 Å) and y (~2.4 Å), respectively. In types C and C′, the molecules are shifted in a diagonal direction. The slip of molecules in type C′ ($x \approx 3.0$, $y \approx 3.0$ Å) is somewhat larger than that in type C ($x \approx 0.7$, $y \approx 1.2$ Å). In type D, the molecules are only a little slipped ($x \approx 0.1$, $y \approx 0.1$ Å), however their molecular axes are twisted with respect to each other. This type has only been found in (TTT)Br[15] and $(TTT)_2[(C_2B_9H_{11})_2Ni](C_6H_3Cl_3)$[16] and is not observed in our salt.

TTT molecules are almost planar in all the salts independent of their ionicity. On the other hand, RO-TCA molecules are not planar. The anion molecule excluding the alkyl group consists of three planar parts, one central C_3O skeleton (plane 1 (P1) in Fig. 3(a) and oxygen atom) and two dicyanomethylene

Table 4 Characteristic parameters of overlap of TTT molecules

Salts	D : A		Overlap mode	x^a/Å	y^a/Å	Interplanar distance/Å	Number of atomic contacts[b]	Overlap integral/10^{-3}
1	1 : 1	Intradimer	B	0.09	2.39	3.32	0 + 8 + 2	−11.79
		Interdimer	C	1.33	0.75	3.46	0 + 0 + 2	9.13
2 (A column)	1 : 1	Intradimer	B	0.07	2.46	3.28	0 + 8 + 4	−12.03
		Interdimer	C	1.25	0.76	3.46	0 + 0 + 0	11.87
2 (B column)	1 : 1	Intradimer	C	1.21	1.13	3.52	0 + 0 + 0	20.70
		Interdimer	C	0.95	0.44	3.55	0 + 0 + 0	7.47
4	1 : 1	Intradimer	C	0.97	0.65	3.40	0 + 0 + 6	18.80
8	1 : 1	Intradimer	B	0.09	2.34	3.34	0 + 6 + 3	9.96
		Interdimer	C′	3.31	3.10	3.59	0 + 0 + 0	2.77
6	3 : 2	Intradimer	A	3.61	0.31	3.26	1 + 0 + 6	−27.44
		Interdimer[c]	C	1.37	1.00	3.46	0 + 0 + 1	7.39

[a]Relative position of molecules (see Fig. 2). [b]Three numbers separated by "+" mean the numbers of S···S, S···C and C···C short atomic contacts, respectively. [c]Between $TTT^{+\bullet}$ and TTT^0.

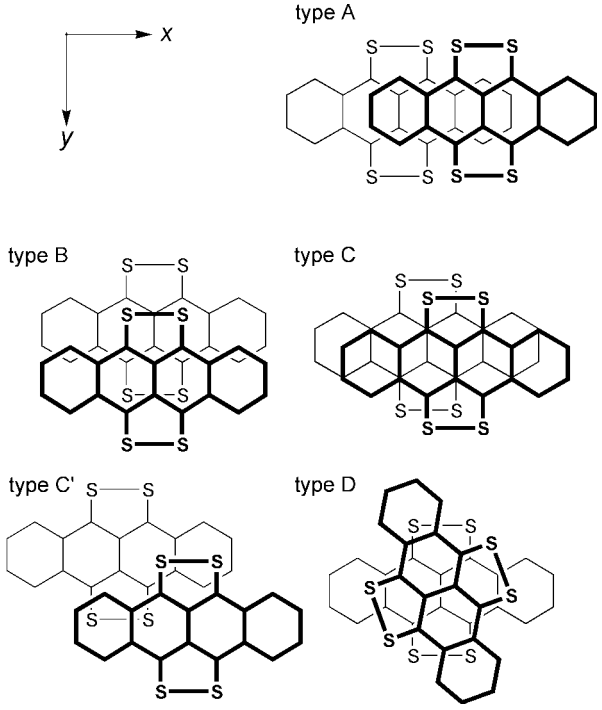

Fig. 2 Overlap patterns of TTT molecules.

$(C(CN)_2)$ groups (plane 2 (P2) and plane 3 (P3) in Fig. 3(a)). The planes are twisted with respect to each other to form a propeller-like structure. The dihedral angles between the planes are different from salt to salt, for example, as shown in Figs. 3(b) and 3(c), which will be discussed below. This demonstrates the flexible nature of RO-TCA.

There are many atomic contacts shorter than the sum of the van der Waals radii[17] between the TTT and anion molecules in the salts. The H···N and S···N contacts are very characteristic. These contacts presumably stabilise the crystal structures, as discussed later.

We describe the crystal structures first, and then examine the molecular structures, overlap modes and interactions between molecules in the following.

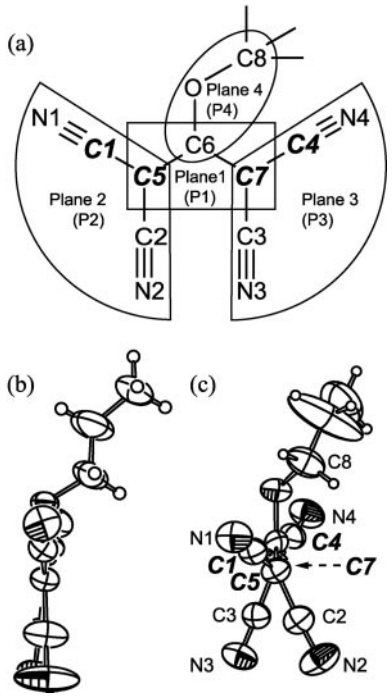

Fig. 3 Molecular structure of RO-TCA anion. (a) Schematic figure and numbering scheme. (b) and (c) Side view of PrO-TCA molecules in **7** and **6**, respectively.

Crystal structures of 1 : 1 salts with segregated columns; (1), (2) and (8). In the 1 : 1 salts except for **4**, the crystal structures are similar to each other in the aspect that the dimerised TTT molecules form segregated columns (Figs. 4(a)–(c)). Compounds **1** and **8** consist crystallographically of one kind of TTT column, while **2** has two kinds.

The main difference between these salts is observed in the intra- and interdimer overlap patterns. As summarised in Table 4, the combinations of the overlap patterns in the TTT columns are different from salt to salt. Another difference among these salts appears as the intermolecular interactions. In **1** and **2**, the calculated overlap integrals between the TTT columns are very small.[18] Consequently, these salts are electronically one-dimensional, though **1** has a layered structure along the *ac*-plane. In **8**, the largest intercolumnar overlap integral is comparable to the interdimer one.[19] Considering the space group, *C*2/*c*, this weak intercolumnar interaction exists in four directions. Therefore, this salt has a weak three-dimensional electronic nature.

Only in **8** do the anion molecules form a columnar structure. The dihedral angles between the central C_3O skeleton of BuO-TCA and the TTT molecules are 8.8–8.9°, which means that all the TTT and BuO-TCA molecules are nearly parallel.[20] In the salt where both donor and anion molecules form individual columnar structures, the cross section of the anion column may become of a similar size to that of the donor column in order to reduce coulombic repulsion between the columns composed of the same kind of molecules. Hence, the nearly parallel structure of TTT and BuO-TCA seems to be caused by the comparable size of the anion to that of the TTT molecule.

Crystal structures of 1 : 1 salts with alternating stacks (4). TTT molecules form dimers and stack with two anions alternately to form $D^{+\bullet}D^{+\bullet}A^{-}A^{-}$ columns along the diagonal $(a-b+c)$ direction (Fig. 4(d)), so that the TTT dimers are almost isolated from each other. The THF molecules are located at the edges of the unit cell. The overlap pattern of TTT molecules is classified into type C.

Crystal structure of 1 : 2 salts (3) and (7). Compounds **3** and **7** are nearly isostructural. Therefore, only the crystal structure of **3** is shown in Fig. 4(e), and that of **7** is available in supplementary Fig. S13.†

One half of the TTT and one RO-TCA molecule are crystallographically independent. Accordingly, the charge of the TTT molecules is deduced to be +2, which is consistent with the optical data described below. In the crystals, two anion molecules are sandwiched by the TTT^{2+} molecules, which makes the TCA skeleton of RO-TCA the most planar structure among all of the RO-TCA salts.

Crystal structure of 3 : 2 salt (6). The asymmetric unit contains one and a half TTT and one PrO-TCA molecules. The bond lengths of two kinds of TTT molecules (TTT(a) and TTT(b)) are evidently different. For example, the mean S–S bond lengths for TTT(a) and TTT(b) are 2.069(3) and 2.090(3) Å, and the S–C bond lengths are 1.737(7) and 1.758(6) Å, respectively. The comparison of the bond lengths with reported ones indicates that the charges on the two TTT molecules are +1 and 0. This charge separation is consistent with optical data (*vide infra*). From now on, TTT(a) and TTT(b) are represented as $TTT^{+\bullet}$ and TTT^{0}, respectively.

$TTT^{+\bullet}$ molecules form dimers similar to the 1 : 1 salt. TTT^{0} (D^{0}) and the dimer of $TTT^{+\bullet}$ ($D^{+\bullet}$) form a segregated column in the sequence $D^{0}D^{+\bullet}D^{+\bullet}D^{0}D^{+\bullet}D^{+\bullet}$ along the *a*-axis (Fig. 4(f)). A similar structure was reported in $(TTT)_3Hg_2Br_6$.[21]

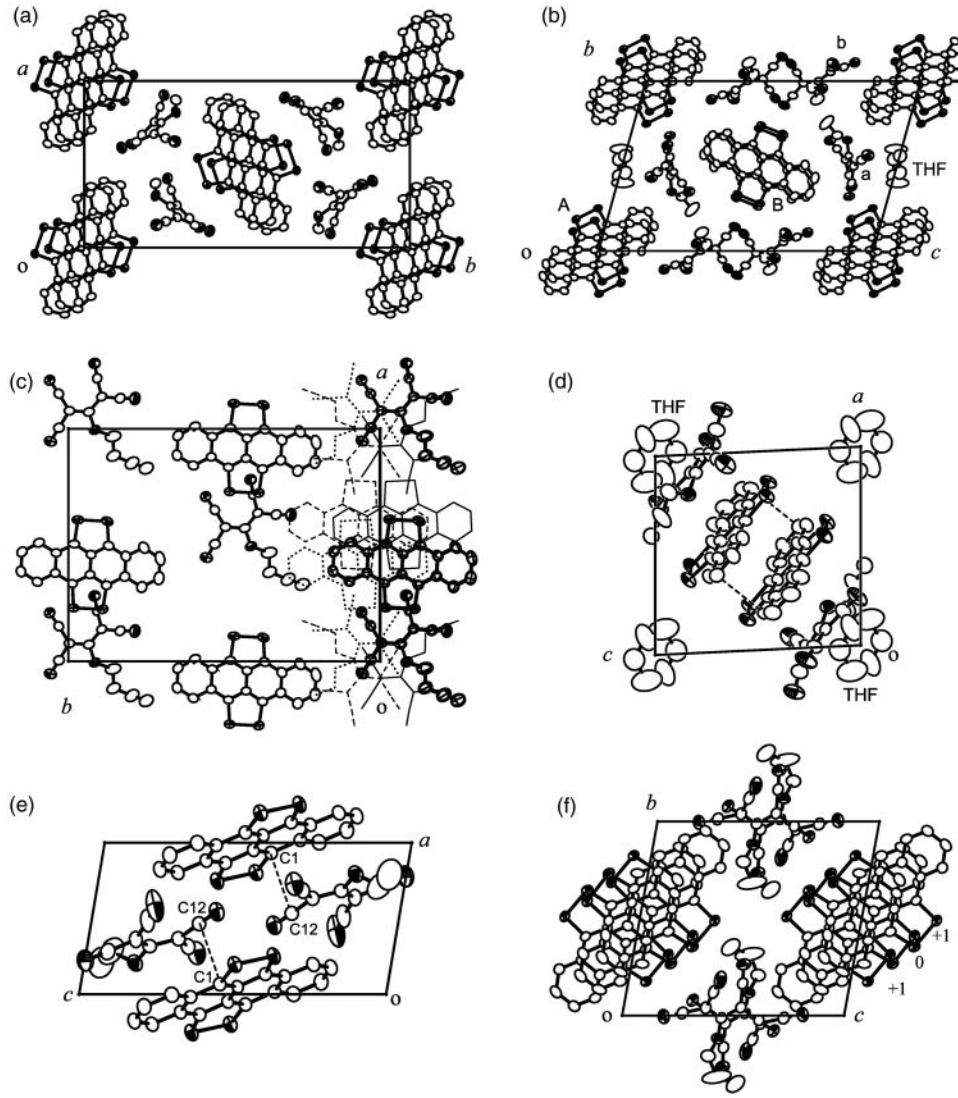

Fig. 4 Crystal structure of TTT salts. (a)(TTT)(MeO-TCA) (**1**) projected along the *c*-axis; (b) (TTT)(EtO-TCA)$(THF)_{0.25}$ (**2**) along the *a*-axis; (c) (TTT)(BuO-TCA) (**8**) along the *c*-axis. Molecules drawn by ellipsoids and solid lines, solid, dotted and dashed lines are located at $z/c \approx 0.1$, 0.4, 0.6 and 0.9, respectively. The region of $y/b > ca.$ 0.25, only molecules near $z/c = 0.1$ are shown for clarity; (d) (TTT)(PrO-TCA)$(THF)_{0.5}$ (**4**) along the *b*-axis; (e) (TTT)$(EtO\text{-}TCA)_2$ (**3**) along the *b*-axis; (f) $(TTT)_3(PrO\text{-}TCA)_2$ (**6**) along the *a*-axis. In (d) and (e), dotted lines indicate short atomic contacts between molecules.

The overlap mode in $TTT^{+\bullet}$ dimer is type A, and that between $TTT^{+\bullet}$ and TTT^0 is type C.

The largest intercolumnar overlap integral along the *b*-axis is only 0.7×10^{-3}, though this is the second largest value next to **8** in our salts. On the other hand, overlap integrals along the *c*-axis are negligible. Therefore, this salt has a very weak two-dimensional electronic nature.

Molecular structures of TTT. The bond lengths of TTT molecules are related to their ionicity (γ). It was reported that the bond lengths of S–S (*a*), S–C (*b*) and C2–C3 (*c*) (inset of Fig. 5) are especially sensitive to the γ values within the range of $0 \leqslant \gamma \leqslant 1$.[1b,22] The lengths of *a* and *b* become shorter and that of *c* becomes longer as TTT is more oxidised, which is consistent with the antibonding nature of *a* and *b* and the bonding nature of *c* in HOMO (inset of Fig. 5).

In Fig. 5, averaged bond lengths with an assumption of D_{2h} symmetry, obtained by our crystal structure analyses where the *R*-values are smaller than 0.080 and the standard deviations of all the three bond lengths are smaller than 0.009 Å, are plotted against the charge on the TTT molecule using filled circles with vertical lines which indicate the standard deviations.[23] Open diamonds indicate reported data within the same criteria.[24] Fig. 5 shows that the TTT^{2+} molecule also fulfils the facts described in the previous paragraph, and that the bond lengths are nearly linearly related to the charge as shown by solid lines that were calculated by least-squares fits. The results of fits are the following: *a* (Å) = $2.0941 - 0.0252\gamma$ ($|r| = 0.973$), *b* (Å) = $1.7604 - 0.0253\gamma$ ($|r| = 0.949$), and *c* (Å) = $1.3988 + 0.0233\gamma$ ($|r| = 0.979$), where *r*'s are correlation coefficients.

The bond lengths of donor molecules are often used to estimate the formal charges. However, it seems to be difficult to distinguish the partially charged TTT molecules by the bond lengths on the basis of Fig. 5, because the difference in the bond lengths between TTT^0 and TTT^{2+} (2.092(2) Å and 2.040(2) Å for *a*, respectively) is rather small compared with that of TTF derivatives. For example, the bond length of the central C=C bond of BEDT-TTF changes from 1.312(12) Å to 1.439(4) Å as the γ value increases from 0 to +2.[25]

The calculated bond lengths by PM3 and RHF/6-31G* methods are also plotted in Fig. 5 by open triangles and crosses, respectively. The calculated results agree with the experimental results within about 0.02 Å. This value is similar to that for BEDT-TTF (0.015 Å).[26] The accuracy of these level calculations may be useful for finding relations between the charges and the bond lengths for TTF derivatives. However, it is not enough for the TTT molecule.

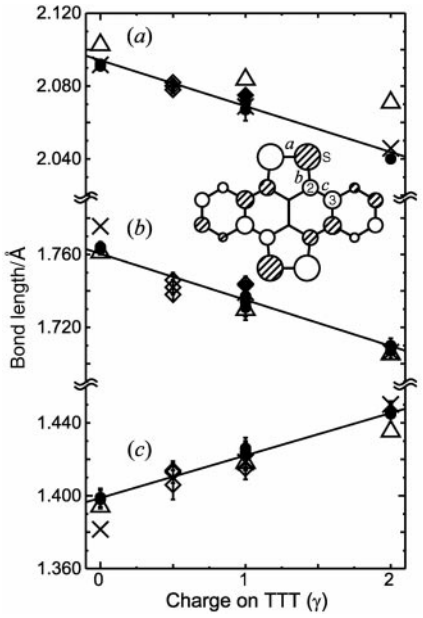

Fig. 5 Relation between the charge and averaged S–S (*a*), S–C (*b*) and C2–C3 (*c*) bond lengths of TTT. Closed circles and open diamonds indicate our experimental results and reported ones, respectively. Lines show results of least-squares fitting. Crosses and open triangles indicate calculated points by RHF/6-31G* and PM3 methods, respectively. Inset shows the HOMO of a TTT molecule calculated by the extended Hückel method, and the position of S, C2, C3, *a*, *b* and *c*.

Interactions between TTT molecules. The S–S bond of the TTT molecule has an antibonding nature in the HOMO, contrary to the case of TTF derivatives in which the coefficients of all the sulfur atoms have the same sign. However, since the sulfur atoms of the TTT molecule have the largest HOMO coefficient, the relative arrangement of S–S bonds between the TTT molecules has a large effect on the intermolecular interactions.

As mentioned before, the overlap modes of TTT molecules are roughly classified into five types (Fig. 2). Type A is observed in most of the highly conducting salts based on not only TTT (*e.g.* $(TTT)_2I_3$[24a,b,27] and $(TTT)_{1.25}Hg_2I_5$[28]) but also TTT derivatives (TST, DMTSA, TMTTeN). This type has the largest overlap integral (*ca.* 25×10^{-3}) in general owing to the smallest interplanar distance and short S···S atomic contacts between molecules. Type B has a small interplanar distance and a large number of S···C atomic contacts; however, it has no S···S atomic contacts. Therefore the overlap integrals of type B (*ca.* 10×10^{-3}) are not so large as those of type A. Type C has a wide range of overlap integrals from 7×10^{-3} to 21×10^{-3} depending on a slight change in the relative position of the molecules. It may be possible that a slight change of the crystal structure composed of type C has a large influence on the physical properties, though such data have not been reported yet. Type C′ has a large slip of the molecule and consequently results in the smallest overlap integral (*ca.* 3×10^{-3}). The overlap integral of type D (*ca.* 10×10^{-3}) is similar to those of type B and most of type C. Summarising the above, type A is the most desirable to obtain highly conducting salts. In our salts, type A is observed only in **6** which is in fact the most conductive, though we cannot directly compare **6** with the other salts because **6** is a unique 3 : 2 salt.

Intercolumnar interaction is rather small in TTT compounds because of the rather large intercolumnar S···S distance. To the best of our knowledge, short S···S contacts between columns are observed only in $(TTT)_2I_3$ (S···S = 3.37 Å)[24a,b,27] among TTT salts. However, the intercolumnar overlap integral is not large (1.3×10^{-3}) owing to the wrong relative orientation of TTT molecules.[29,30] In our case, somewhat large intercolumnar overlap integrals are observed only in **6** and **8**.

If larger chalcogen atoms are introduced to the donor molecule, short chalcogen···chalcogen atomic contacts between columns are expected. Although the symmetries of the HOMO of the donor molecules are the same as that of the TTT molecule, the short atomic contacts bring about significant intercolumnar overlap integrals and three-dimensional character. Actually, $(TST)_2Cl$[29] and some of TMTTeN salts[31] are reported to have three-dimensional character.

Molecular structures of RO-TCA. Although the optimised structure of the TCA skeleton of RO-TCA$^-$ by MO calculations is almost planar, the real RO-TCA$^-$ molecule in the solid takes a non-planar structure as described before. The dihedral angle between the two dicyanomethylene groups (P2 and P3 in Fig. 3(a)) varies in a wide range from 8.3° (**7**) to 48.4° (**6**) shown in Figs. 3(b) and 3(c). Because of this flexibility, polymorphism of the salts may be realised. The flexibility also seems to play an important role in bringing about structural similarity of the packing of donor molecules within the given stoichiometries.

In order to know more about the structural features of RO-TCA, some of the dihedral angles between planes are plotted in Fig. 6 against the torsion angle of C1–C5–C7–C4 (Fig. 3(a)). Filled circles, open squares and filled triangles in Fig. 6(a) show the observed dihedral angles between P1 and P2, P1 and P3, and P2 and P3 in Fig. 3(a), respectively.[32] The parameters obtained from the optimised geometries by RHF/6-31G* calculations with the fixed torsion angles are also indicated by solid, dashed and dotted lines for each of the dihedral angles. Fig. 6(b) shows the relation between the torsion angle and the dihedral angles between P1 and P4. Open diamonds and the solid line show the experimentally observed dihedral angles and the optimised ones by the RHF/6-31G* calculation, respectively. In both Figs. 6(a) and (b), the calculated results approximately agree with the experimental ones in all the four dihedral angles except for the dihedral angle of P1–P4 in **8**.[33] These agreements between the experimental and the calculated results reveal that the RO-TCA molecule tends to become the most stable structure within the given torsion angle, which seems to be determined by mainly atomic contacts described below during the formation of the crystal.

The deviation of the dihedral angle of P1–P4 in **8** seems to come from the columnar structure of BuO-TCA molecules in the salt. It suggests that although the molecular structure of RO-TCA is fundamentally restrained by the torsion angle, RO-TCA has the flexibility to change its own structure in order to achieve better packing in some cases.

Finally in this section, we discuss the flexibility of RO-TCA numerically on the basis of MO calculations. The energy difference between the fully optimised structure and the

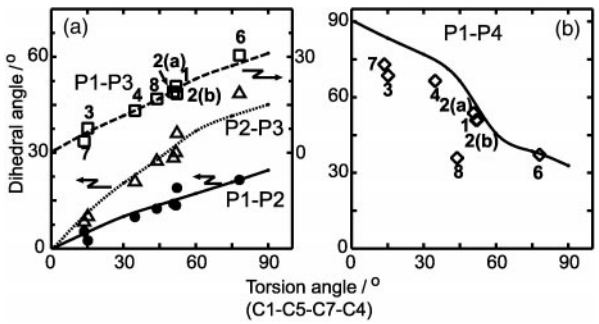

Fig. 6 Dihedral angles between the planes of RO-TCA molecules against the torsion angle C1–C5–C7–C4. (a) Filled circles: dihedral angles between planes 1 and 2; open squares: between planes 1 and 3; filled triangles: between planes 2 and 3. Solid, dashed, dotted and dash-dotted lines indicate calculated angles by RHF/6-31G* methods. (b) Dihedral angles between planes 1 and 4 (open diamonds). Solid line indicates calculated angles by RHF/6-31G* methods.

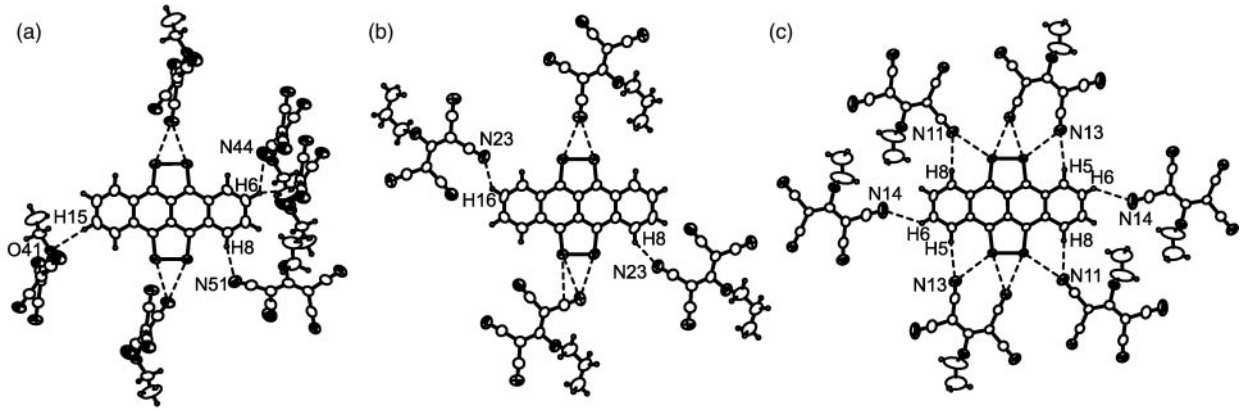

Fig. 7 Short atomic contacts between TTT and RO-TCA molecules. (a) TTT(A) molecule in **2**; (b) in **4**; (c) in **3**.

optimised structure with the fixed torsion angle (C1–C5–C7–C4) of 90° is estimated to be 2.3 and 1.9 kcal mol^{-1} by RHF/6-31G* and PM3 calculations, respectively. Between the optimised structures with a torsion angle of 0° and that of 90°, there is no local maximum of energy. This energy difference is as small as the rotation barrier of a C–C bond in an ethane molecule (3 kcal mol^{-1}). This result emphasises that RO-TCA anions can modify their molecular shapes to accommodate in the crystals.

Interactions between TTT and RO-TCA. Atomic contacts between hydrogen or sulfur atoms of TTT and nitrogen atoms of anions are observed commonly in these salts. Typical cases are shown in Fig. 7 by dashed lines. The shortest H···N and S···N distances are 2.37(3) Å (in **2**) and 2.871(4) Å (in **2**), respectively, considerably shorter than the sum of the van der Waals radii (H: 1.20; S: 1.80; N: 1.55 Å).[17]

The short atomic contacts between H and N or O atoms seem to be a kind of C–H···X type weak hydrogen bonds,[34] characterised by shorter C···X distances than about 4.0 Å and larger C–H···X angles than about 110° as summarised in supplementary Table S8.

The pattern of S···N contacts in which one N atom and two S atoms form a nearly isosceles triangle is the most frequently observed as shown in Fig. 7 and supplementary Fig. S16. These S···N contacts can be mainly attributed to coulombic interaction because of the following reasons. (1) This pattern can take little advantage of an overlap of MO because of the antibonding nature of S–S bonds. (2) The interactions are not directional; that is, the angles of S···N≡C and the dihedral angles between the TTT molecule and dicyanomethylene group of RO-TCA are obviously different from salt to salt. For example, the S···N≡C angle ranges from 75.3 to 163.4° in **4**; the dihedral angles between the TTT molecules and dicyanomethylene groups of RO-TCA are 82–85° in **2** and 3–9° in **4**. (3) The charge distribution calculated by RHF/6-31G* shown in supplementary Fig. S17 demonstrates that the S atoms of TTT and the N atoms of RO-TCA$^-$ have opposite charges, positive and negative, respectively.

To illustrate the strength of the coulombic interaction relative to the van der Waals interaction, the Coulomb and the van der Waals energies are roughly calculated as follows. We chose the configuration of the upper part of Fig. 7(b) (in **4**), which is evaluated to have the smallest influence of H···N contacts among the salts. The Coulomb energy of the nearly isosceles triangle S···N···S interaction in that configuration is estimated as 32 kcal mol^{-1} by simple summation of the Coulomb energy ($-qq'/r$),[35] using the calculated charge distribution of TTT$^{+\bullet}$ and MeO-TCA$^-$. To estimate the van der Waals energy between TTT and RO-TCA molecules, an RHF/6-31G* calculation was applied to obtain the total energy of a TTT^0 and PrO-TCA$^-$ pair in the same orientation as used in the Coulomb energy calculation. The total energy was compared to that of isolated TTT^0 and PrO-TCA$^-$ molecules to give the cohesive energy of 3.2 kcal mol^{-1}. Thus the coulombic interaction between two S atoms of TTT$^{+\bullet}$ and one N atom of RO-TCA$^-$ is evaluated to be about ten times as strong as the van der Waals interaction. The energy of the interaction is also larger than that needed to modify the shape of the RO-TCA molecule.

In TTT^0, the H atoms bear more positive charge than the S atoms, as far as the MO calculation of the isolated molecule is

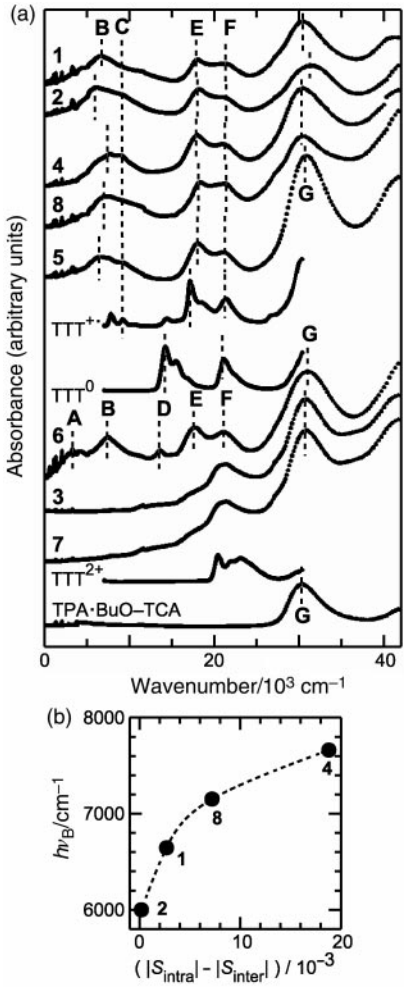

Fig. 8 (a) Optical spectra of the salts. TTT^0: $CHCl_3$ solution; TTT$^{+\bullet}$: ethanol solution of (TTT)Cl·H_2O; TTT^{2+}: H_2SO_4 solution of $(TTT)(HSO_4)_2$; salts **1** to **8** and TPA·BuO-TCA: KBr dispersed pellets. For bands A–G, see text. (b) Energy of band B ($h\nu_B$) as a function of $|S_{intra}| - |S_{inter}|$. The dashed line is a guide to the eye.

concerned. Furthermore, H···N contacts are generally shorter than S···N contacts. Therefore, H···N contacts gain more Coulomb cohesive energies than S···N contacts.[36] In fact, PM3 calculation ascertains that the configuration of TTT^0 and RO-TCA^- with H···N contacts is more stable than that with S···N contacts. On the contrary, S···N contacts are observed in **6** while H···N contacts are not, as shown in supplementary Fig. S16(f). This indicates that the factors that determine the packing motifs in the crystal are not simple.

3.3 Physical properties of TTT salts

Optical properties. Optical spectra of the salts are shown in Fig. 8(a). Solution spectra of TTT^0 (in $CHCl_3$), $TTT^{+\bullet}$ (in methanol) and TTT^{2+} (in H_2SO_4) are also presented, which agree with those reported.[22a,37] On the basis of the absorption spectra, the TTT salts can be efficiently characterised as follows.

The 1 : 1 salts (**1**, **2**, **4**, **8**) exhibit the lowest energy band around $7 \times 10^3\ cm^{-1}$ (labelled band B) which corresponds to the admixture of the intramolecular transition of $TTT^{+\bullet}$ and the charge transfer one between two $TTT^{+\bullet}$ molecules, namely $2TTT^{+\bullet} \rightarrow TTT^0 + TTT^{2+}$. Since the latter seems to be stronger than the former, the latter mainly influences the positions of band B. Fig. 8(b) shows the energy of band B ($h\nu_B$) as a function of the difference of the absolute values of the intradimer overlap integral (S_{intra}) and interdimer overlap integral (S_{inter}), which is related to the split of the HOMO band. When $|S_{intra}| - |S_{inter}|$ becomes larger, the band B appears at higher energy. The band B of **4** is located at the highest energy, which corresponds to a pure intradimer transition of $(TTT^{+\bullet})_2$, because **4** consists of almost isolated $TTT^{+\bullet}$ dimers. The $h\nu_B$ value of an isolated dimer with two electrons is represented as[38]

$$h\nu_B = U/2 + (U^2/4 + 4t^2) \quad (1)$$

where U is on-site Coulomb repulsion and t is the transfer integral between molecules. Concerning the size and the polarisability of the molecule, and the interplanar distance, effective U (U_{eff}) should be used in the solid. Using observed $h\nu_B$ and t evaluated from S_{intra} by the relation of $t = ES_{intra}$ ($E = -10$ eV),[10] U_{eff} is estimated to be 0.8 eV. This value is a little larger than that of BEDT-TTF ($U_{eff} \approx 0.7$ eV)[39] and considerably smaller than that of TTF ($U_{eff} \approx 1.25$ eV).[40]

In addition to band B, the 1 : 1 salts have optical bands C, E and F as shown in Fig. 8(a), which are ascribed to the intramolecular transitions of $TTT^{+\bullet}$. The absorption band G is the superposition of those of $TTT^{+\bullet}$ and RO-TCA^-, which is almost independent of the alkyl group and conformation of the molecule.

Salt **5**, whose stoichiometry is unknown, has almost the same absorption bands as those of the 1 : 1 salts with columnar structures. This implies that **5** is most plausibly a 1 : 1 salt and has a columnar structure.

The 3 : 2 salt (**6**) has additional absorption bands to those of the 1 : 1 salts around 14×10^3 (labelled band D) and $3.5 \times 10^3\ cm^{-1}$ (labelled band A), which correspond to the intramolecular transition of TTT^0 and the charge transfer one between TTT^0 and $TTT^{+\bullet}$, $TTT^0 + TTT^{+\bullet} \rightarrow TTT^{+\bullet} + TTT^0$, respectively. These confirm that there is a charge separation of TTT^0 and $TTT^{+\bullet}$ in agreement with the molecular structures described above.

The 1 : 2 salts (**3**, **7**) exhibit the optical band ascribable to the intramolecular transition of either TTT^0, $TTT^{+\bullet}$ or TTT^{2+} around $20 \times 10^3\ cm^{-1}$. However, no clear appearance of bands assignable to TTT^0 (band D) and $TTT^{+\bullet}$ (bands C and E) indicates that the charge of TTT molecule is +2.

IR spectra are also utilised to identify the component species in the TTT salts.[41] The wavenumbers of peaks corresponding to TTT molecules in the PrO-TCA salts (**4**, **5**, **6** and **7**) are summarised together with those of TTT^0, $TTT^{+\bullet}$ and TTT^{2+} salts with inorganic anions in supplementary Table S9. Although some peaks are hard to see owing to the overlap with those of the anion, the comparison of IR spectra affords the same results as that of UV-Vis-NIR spectra.

Table 5 Resistivities at room temperature and activation energies for conduction

Salts		ρ_{RT}/Ωcm	E_a/eV
1 : 1	**1**	1.4×10^4	0.30
	2	3.5×10^5	0.35
	4	4.3×10^6	0.27
	5	1.7×10^5	0.32
	8	9.9×10^6	0.33
1 : 2	**3**	1.1×10^6	0.27
	7	1.2×10^6	0.34
3 : 2	**6**	2.1×10^3	0.33

Resistivity and magnetic susceptibility. As expected from the structural data, all the salts are semiconductors. Electrical resistivities and activation energies are summarised in Table 5. Semiconducting behaviour is very natural for the salts with alternating stacks. In the salt with segregated columns, the dimerised structures in the 1 : 1 salts and the triad one in the 3 : 2 salts give rise to an energy gap at the Fermi level. Within the tight-binding approximation, the energy gaps in the 1 : 1 salts with one-dimensional segregated columns are estimated as $2(|t| - |t'|)$, where t and t' are intradimer and interdimer transfer integrals, respectively. Therefore, the E_a values are expected to be related to $|S_{intra}| - |S_{inter}|$. However, in contrast to the case of the optical band B, we cannot find obvious relations between E_a and $|S_{intra}| - |S_{inter}|$.

The 1 : 1 and 3 : 2 salts are paramagnetic following the Curie law down to 2 K (shown in supplementary Fig. S18). However, the spin densities were only 0.2–2.3% of the complexes so can be attributed to crystal defects or impurities. Only **4** shows slight deviation from Curie behaviour at high temperature which can be attributed to singlet–triplet excitation with an energy gap of *ca.* 1240 K. Similar behaviour is not observed in the other salts presumably because the energy gaps are much larger than that in **4**.

4 Conclusion

We prepared eight TTT salts with a series of the flexible RO-TCA^- anions (R = Me, Et, Pr^n, Bu^n). The structural aspects including intermolecular interaction and atomic contacts are discussed in detail. It was observed that the anion molecules varied their molecular shape to fit in the environment in the crystals. The use of the flexible anions produces novel crystal structures, which have alternating stacks of TTT and anion molecules. It should be emphasised that two of them are composed of TTT^{2+}, whose structure is determined for the first time. As for the physical properties, the salts are simply non-magnetic semiconductors.

The flexibility of the anion shows two features about a series of the salts. The first is polymorphism with multiple stoichiometries. The second is that, within a given stoichiometry, the crystal structures are similar to each other with one exception (salt **4**), even changing the alkyl group. In addition to these features, N atoms of the anion have many atomic contacts with H or S atoms of TTT, which seem to play an important role in building the crystal structures. On the basis of these points, the anion series is also expected to bring about novel cation radical salts with the other donor molecules.

Acknowledgements

The authors would like to thank Professor R. P. Shibaeva for providing unpublished data about crystal structures of TTT salts. This work was in part supported by a Grant-in-Aid for Scientific Research from Ministry of Education, Science, Sports, Culture, and Technology, Japan, a fund for "Research for the Future" from Japan Society for Promotion of Science and a fund for the International Joint Research Grant Program of the New Energy and Industrial Technology Development Organization (NEDO).

References

1 (*a*) I. F. Shchegolev and E. B. Yagubskii, in *Extended Linear Chain Compounds*, ed. J. S. Miller, Plenum Press, New York, 1982, Vol. 2, p. 385; (*b*) R. P. Shibaeva, in *Extended Linear Chain Compounds*, ed. J. S. Miller, *Plenum Press*, New York, 1982, Vol. 2, p. 435.

2 K. Takimiya, A. Ohnishi, Y. Aso, T. Otsubo, F. Ogura, K. Kawabata, K. Tanaka and M. Mizutani, *Bull. Chem. Soc. Jpn.*, 1994, **67**, 766.

3 O. H. Le Blanc, Jr., *J. Chem. Phys.*, 1965, **42**, 4307.

4 (*a*) H. Yamochi, T. Tsuji, G. Saito, T. Suzuki, T. Miyashi and C. Kabuto, *Synth. Met.*, 1988, **27**, A479; (*b*) H. Yamochi, A. Konsha, G. Saito, K. Matsumoto, M. Kusunoki and K. Sakaguchi, *Mol. Cryst. Liq. Cryst.*, 2000, **350**, 265; (*c*) G. Saito, S. Sekizaki, A. Konsha, H. Yamochi, K. Matsumoto, M. Kusunoki and K. Sakaguchi, *J. Mater. Chem.*, 2001, **11**, 364.

5 Some parts of the results were briefly reported in the following papers: (*a*) H. Yamochi, C. Tada, S. Sekizaki, G. Saito, M. Kusunoki and K. Sakaguchi, *Mol. Cryst. Liq. Cryst.*, 1996, **284**, 379; (*b*) S. Sekizaki, H. Yamochi and G. Saito, *Synth. Met.*, 1999, **102**, 1711.

6 C. Marschalk, *Bull. Soc. Chim. Fr.*, 1952, 147.

7 E. P. Goodings, D. A. Mitcahard and G. Owen, *J. Chem. Soc., Perkin Trans. 1*, 1972, 1310.

8 (*a*) W. J. Middleton and V. A. Engelhardt, *J. Am. Chem. Soc.*, 1958, **80**, 2788; (*b*) W. J. Middleton, E. L. Little, D. D. Coffman and V. A. Engelhardt, *J. Am. Chem. Soc.*, 1958, **80**, 2795.

9 CrystanGM 6.3.3, MAC Science Co. Ltd., 1995.

10 T. Mori, A. Kobayashi, H. Kobayashi, G. Saito and H. Inokuchi, *Bull. Chem. Soc. Jpn.*, 1984, **57**, 627.

11 MOPAC97 Co. Ltd. Fujitsu and J. J. P. Stewart, *J. Comput. Chem.*, 1989, **10**, 209.

12 The open shell RHF (ROHF) method was used for $TTT^{+\bullet}$.

13 (*a*) Gaussian 94, Revision D.4, Gaussian, Inc., Pittsburgh PA, 1995; (*b*) Gaussian 98, Revision A.9, M. J. Frisch, G. W. Trucks, H. B. Schlegel, G. E. Scuseria, M. A. Robb, J. R. Cheeseman, V. G. Zakrzewski, J. A. Montgomery Jr., R. E. Stratmann, J. C. Burant, S. Dapprich, J. M. Millam, A. D. Daniels, K. N. Kudin, M. C. Strain, O. Farkas, J. Tomasi, V. Barone, M. Cossi, R. Cammi, B. Mennucci, C. Pomelli, C. Adamo, S. Clifford, J. Ochterski, G. A. Petersson, P. Y. Ayala, Q. Cui, K. Morokuma, D. K. Malick, A. D. Rabuck, K. Raghavachari, J. B. Foresman, J. Cioslowski, J. V. Ortiz, A. G. Baboul, B. B. Stefanov, G. Liu, A. Liashenko, P. Piskorz, I. Komaromi, R. Gomperts, R. L. Martin, D. J. Fox, T. Keith, M. A. Al-Laham, C. Y. Peng, A. Nanayakkara, M. Challacombe, P. M. W. Gill, B. Johnson, W. Chen, M. W. Wong, J. L. Andres, C. Gonzalez, M. Head-Gordon, E. S. Replogle and J. A. Pople, Gaussian, Inc., Pittsburgh PA, 1998.

14 This result seems to be consistent with that the pK_a values of H·TCA and H·PCA are smaller than that of hydrochloric acid; see; R. H. Boyd, *J. Phys. Chem.*, 1963, **67**, 737.

15 R. P. Shibaeva, V. F. Kaminskii, O. N. Eremenko, E. B. Yagbuskii and M. L. Khidekel, *Kristallografiya*, 1980, **25**, 60.

16 P. A. Chetcuti, W. Hofherr, A. Liégard, G. Rihs, H. Keller and D. Zech, *Organometallics*, 1995, **14**, 666.

17 A. Bondi, *J. Phys. Chem.*, 1964, **68**, 441.

18 In **1**, the smallest overlap integral of HOMOs in the column is 9.1×10^{-3}, while the largest intercolumnar one is 0.09×10^{-3}. In **2**, the donor columns are separated from each other by solvent and the anion molecules. Therefore there are no significant intercolumnar overlap integrals.

19 Intra- and interdimer overlap integrals are 10.0×10^{-3} and 2.8×10^{-3}, respectively, while the largest overlap integral between neighbouring TTT columns is 1.4×10^{-3}.

20 Dihedral angles between the central C_3O skeleton of RO-TCA and TTT molecules in the other salts with columnar structures of TTT molecules are the following: 47.4 and 74.6° in **1**, from 34.5 to 88.1° in **2**, about 30.2° in **6**.

21 R. P. Shibaeva and V. F. Kaminskii, *Kristallografiya*, 1983, **28**, 296.

22 (*a*) Á. I. Kiss, M. Kertész, P. Cársky and H. Wedel, *Tetrahedron*, 1979, **35**, 515; (*b*) J. -P. Boutique, J. Riga, J. J. Verbist, J. G. Fripiat and J. Delhalle, *Mol. Cryst. Liq. Cryst.*, 1983, **101**, 175.

23 **1**, **2**, **8**, **3** and **7** satisfy our criteria. The structure of neutral TTT was redetermined in our laboratory, because reported data (O. Dideberg and J. Toussaint, *Acta Crystallogr., Sect. B*, 1974, **30**, 2481) do not satisfy the criteria (the *R*-value is 0.13). Unit cell parameters determined by us, $a = 9.881(2)$, $b = 18.212(2)$, $c = 3.9620(3)$ Å, $\alpha = 87.638(7)$, $\beta = 79.597(8)$, $\gamma = 96.582(7)°$ and $V = 695.2(2)$ Å^3, are identical within an experimental error to the reported data. Number of observed reflections 1959 ($I > 3.00\sigma(I)$), number of refined parameters 231, *R*-value 0.028. Hydrogen atoms were determined by differential synthesis.

24 The data of $TTT^{+\bullet}$ were taken from ref. 15. Those of $TTT^{0.5+}$ from ref. 16 and (*a*) D. L. Smith and H. R. Luss, *Acta Crystallogr., Sect B*, 1977, **33**, 1744; (*b*) C. Lowe-Ma, R. Williams and S. Samson, *J. Chem. Phys.*, 1981, **74**, 1966.

25 L.-K. Chou, M. A. Quijada, M. B. Clevenger, G. F. de Oliveira, K. A. Abboud, D. B. Tanner and D. R. Talham, *Chem. Mater.*, 1995, **7**, 530.

26 E. Demiralp and W. A. Goddard III, *J. Phys. Chem.*, 1994, **98**, 9781; in the paper, the calculation was performed with a higher level basis set (6-31G**) than in our paper.

27 (*a*) R. P. Shibaeva and V. F. Kaminskii, *Kristallografiya*, 1978, **23**, 499; (*b*) P. A. Filhol, J. Gaultier, C. Hauw, B. Hilti and C. Mayer, *Acta Crystallogr., Sect. B*, 1982, **28**, 2577.

28 (*a*) V. F. Kaminskii, E. E. Kostuchenko, R. P. Shibaeva, E. B. Yagbuskii and A. V. Zvarykina, *J. Phys. Colloq.*, 1983, **C3**, 1167; (*b*) R. P. Shibaeva, personal communication; she mentioned that the stoichiometry of $(TTT)_{1.25}Hg_2I_5$ has some ambiguity.

29 T. Mori, A. Kobayashi, Y. Sasaki and H. Kobayashi, *Bull. Chem. Soc. Jpn.*, 1983, **56**, 3376; in the paper, single-ζ Slater components without 3d-orbitals of the sulfur atoms are used in extended Hückel calculations.

30 Our preliminary calculation indicates that the intercolumnar overlap integral becomes as much as 7×10^{-3}, if the relative position of TTT molecules is appropriate. However, in such cases, molecular packing in the crystal seems to be rather loose.

31 (*a*) E. Arai, H. Fujiwara, H. Kobayashi, A. Kobayashi, K. Takimiya, T. Otsubo and F. Ogura, *Inorg. Chem.*, 1998, **37**, 2850; (*b*) A. Kobayashi, M. Nakata, E. Arai, H. Fujiwara, H. Kobayashi, K. Takimiya, T. Otsubo and F. Ogura, *Synth. Met.*, 1999, **103**, 1865; (*c*) E. Ojima, B. Z. Narymbetov, H. Fujiwara, H. Kobayashi, A. Kobayashi, K. Takimiya, T. Otsubo and F. Ogura, *Chem. Lett.*, 1999, 845.

32 The torsion angle of C1–C5–C7–C4 is generally larger than that of C2–C5–C7–C3 and the dihedral angle between P2 and P3, though the planes keep almost planar structures; the largest shift of an atom from the least-squares plane is only about 0.025 Å. This apparent discrepancy comes from the geometrical reason that the positions of C5 and C7 are deviated from the opposite planes, P3 and P2, respectively. For example, in **6**, C5 and C7 locate 0.57 and 0.33 Å away from the P3 and P2, respectively (see Fig. 3(c)).

33 The results of PM3 calculation are almost the same as those of RHF/6-31G* calculation for P1–P2, P1–P3 and P2–P3. However, as for P1–P4, RHF/6-31G* calculation provides better results than the PM3 method.

34 (*a*) G. R. Desiraju, *Acc. Chem. Res.*, 1991, **24**, 290; (*b*) T. Steiner, *Cryst. Rev.*, 1996, **6**, 1; (*c*) C. E. Marjo, M. L. Scudder, D. C. Craig and R. Bishop, *J. Chem. Soc., Perkin Trans. 2*, 1997, 2099; (*d*) P. J. Langley, J. Hulliger, R. Thaimattam and G. R. Desiraju, *New. J. Chem.*, 1998, **22**, 1307; (*e*) V. R. Thalladi, A. Gehrke and R. Boese, *New J. Chem.*, 2000, **24**, 463.

35 When all the atoms of TTT and PrO-TCA molecules are considered, the summation of the Coulomb energy is estimated as 41 kcal mol^{-1}.

36 When the H···N distance is assumed to be 2.65 Å, Coulomb energies per H···N contact are calculated as 15, 17 and 19 kcal mol^{-1} for TTT^0, $TTT^{+\bullet}$ and TTT^{2+}, respectively. When the S···N distance is assumed to be 3.00 Å, Coulomb energies per S···N contact are calculated as 9, 16 and 23 kcal mol^{-1} for TTT^0, $TTT^{+\bullet}$ and TTT^{2+}, respectively.

37 (*a*) Y. Matsunaga, *Bull. Chem. Soc. Jpn.*, 1972, **45**, 770; (*b*) K. Kamarás and G. Grüner, *Solid State Commun.*, 1979, **30**, 277.

38 C. S. Jacobsen, *Highly Conduting Quasi-One-Dimensional Organic Crystals (Semiconductors and Semimetals vol. 27)*, ed. E. Conwell, Academic Press, San Diego, 1988, p. 293.
39 H. Tajima, M. Tamura, H. Kuroda, T. Mori and H. Inokuchi, *Bull. Chem. Soc. Jpn.*, 1990, **63**, 538.
40 J. B. Torrance, B. A. Scott, B. Welber, F. B. Kaufman and P. E. Seiden, *Phys. Rev. B*, 1979, **19**, 730.
41 (*a*) E. A. Perez-Alubuerne, H. Johnson Jr. and D. J. Trevoy, *J. Chem. Phys.*, 1971, **55**, 1547; (*b*) Y. Matsunaga and K. Takayanagi, *Bull. Chem. Soc. Jpn.*, 1980, **53**, 2796.